The Astrophysical Journal, 980:241 (11pp), 2025 February 20 https://doi.org/10.3847/1538-4357/adadef

GRB 221009A and the Apparently Most Energetic Gamma-Ray Bursts

Jean-Luc Atteia[1], Laurent Bouchet[1], Jean-Pascal Dezalay[1], Francis Fortin[1], Olivier Godet[1], Sébastien Guillot[1], Alain Klotz[1], Frédéric Daigne[2,4], Robert Mochkovitch[2], and Damien Turpin[3]
[1] IRAP, Université de Toulouse, CNRS, CNES, UPS, Toulouse, France
[2] Sorbonne Université, CNRS, UMR 7095, Institut d'Astrophysique de Paris, 98 Bis bd Arago, 75014, Paris, France
[3] Université Paris-Saclay, Université Paris Cité, CEA, CNRS, AIM, Gif-sur-Yvette, France
[4] Institut Universitaire de France, Ministère de l'Enseignement Supérieur et de la Recherche, 1 rue Descartes, 75231, Paris Cedex F-05, France
Received 2024 August 21; revised 2025 January 6; accepted 2025 January 22; published 2025 February 19

Abstract

Gamma-ray bursts (GRBs) are often referred to as the most luminous explosions in the Universe, due to their short and highly luminous prompt emission. This apparent luminosity, however, does not reflect the true energy budget of the prompt emission, which is strongly beamed. Accurate estimations of the energy radiated during the prompt phase require taking the geometry of GRB jets into account, which remains poorly known. Nevertheless, one may establish the distribution of well-measured quantities, like $E_{\rm iso}$, the GRB isotropic equivalent energy, which encrypts crucial information about GRB jets, with the aim of providing constraints on the jet's radiated energy. In this work, we study the bright end of the GRB isotropic equivalent energy distribution (hereafter called "apparent energy"), using an updated sample of 185 apparently energetic GRBs with $E_{\rm iso} \geqslant 10^{53}$ erg. This new sample includes GRB 221009A, allowing us to discuss this apparently superenergetic GRB in the context of the general $E_{\rm iso}$ distribution of long GRBs. We describe the construction of the sample and compare three fits of the $E_{\rm iso}$ distribution with a simple power law, a cutoff power law, and a broken power law. Our study confirms the existence of a cutoff around $E_{\rm iso} = 4 \times 10^{54}$ erg, even when GRB 221009A is included in the sample. Based on this finding, we discuss the possible reasons behind the rapid decrease in the number of apparently energetic gamma-ray bursts beyond $E_{\rm iso} = 4 \times 10^{54}$ erg and the interpretation of GRB 221009A, the most apparently energetic GRB detected to date, in this context.

Unified Astronomy Thesaurus concepts: Gamma-ray bursts (629)

Materials only available in the online version of record: machine-readable table

1. Introduction

Gamma-ray bursts (GRBs) appear as short and extremely luminous flashes of gamma rays, with an isotropic equivalent bolometric luminosity that can reach or exceed 10^{53} erg s^{-1} during the brief duration of the prompt emission. Integrating this luminosity over the duration of the prompt emission gives $E_{\rm iso}$, the *isotropic equivalent energy*, which can also reach extreme values, over 10^{54} erg (S. R. Kulkarni et al. 1998; S. B. Cenko et al. 2010; D. D. Frederiks et al. 2013; J. L. Atteia et al. 2017).

These large apparent energies are due to the particular geometry of GRBs whose prompt emission is produced in ultrarelativistic jets that are highly collimated (J. E. Rhoads 1997; D. A. Frail et al. 2001). Given this geometry, $E_{\rm iso}$ does not represent the total energy radiated in gamma rays but the energy per solid angle emitted *in our direction*. Considering jets with typical opening angles of a few degrees (e.g., D. A. Frail et al. 2001; P. Beniamini & E. Nakar 2019; W. Zhao et al. 2020) reduces the prompt energy output by a large factor, typically 100–1000, leading to energy budgets of few times 10^{51} erg, comparable with the kinetic energy of typical core-collapse supernovae (e.g., S. E. Woosley & J. S. Bloom 2006).

Despite its dependence on the observer's viewing angle, the study of the $E_{\rm iso}$ distribution presents some interest: first, $E_{\rm iso}$ is available for several hundreds of GRBs, allowing statistical studies and second, it conveys useful information on GRB jets, especially on its bright end, which is shaped by the most luminous jets seen on axis and little impacted by orientation effects. In this article, we revisit the bright end of the long GRBs (LGRBs) isotropic energy distribution after the detection of GRB 221009A, whose isotropic energy exceeded all previous measurements. Our GRB sample is about 2 times larger than in our previous work (J. L. Atteia et al. 2017, hereafter A17). To stress the dependence of $E_{\rm iso}$ on the viewing angle, we use in the following the term "apparent energy" to qualify this quantity.

After constructing a sample of 185 LGRBs with $E_{\rm iso} \geqslant 10^{53}$ erg in Section 2, we confirm in Section 3 the existence of a cutoff at a few $\geqslant 10^{54}$ erg (A17; A. Tsvetkova et al. 2017; L. Lan et al. 2023), and we demonstrate that the existence of GRB 221009A does not modify this conclusion. In the last section (Section 4), we address the question of whether the exceptional $E_{\rm iso}$ of GRB 221009A makes it an exceptional burst, and we discuss the possible origin of the observed $E_{\rm iso}$ cutoff.

Throughout this paper, we use a flat Λ-CDM model, with the cosmological parameters measured by the Planck collaboration (Planck Collaboration et al. 2014), $H_0 = 67.3$ km s^{-1} Mpc^{-1}, and $\Omega_{\rm m} = 0.315$ to keep the consistency with the work of A. Tsvetkova et al. (2017), A. Tsvetkova et al. (2021), and S. Poolakkil et al. (2021). Unless otherwise specified, errors are given at the 1σ level.

2. Sample Construction

Our sample includes 185 GRBs with $E_{\rm iso} \geqslant 10^{53}$ erg detected up to the end of 2023, including GRB 221009A. This is about

40% of the 450 known GRBs with a redshift. The choice of GRBs with $E_{\rm iso} \geqslant 10^{53}$ erg is a compromise between two requirements. On one side, a dynamic range in $E_{\rm iso}$ covering more than 1 order of magnitude and a number of GRBs > 100 is needed to statistically characterize the bright end of the energy distribution. On the other hand, the choice to have a nearly volume complete sample, even if this last requirement is not strictly necessary for this study. In the following, we call "apparently energetic GRBs," GRBs with $E_{\rm iso} \geqslant 10^{53}$ erg and "apparently very energetic GRBs," those with $E_{\rm iso} \geqslant 10^{54}$ erg.

Since the computation of $E_{\rm iso}$ requires measuring the redshift and the spectrum of the prompt emission, our sample contains essentially GRBs detected by both the Neil Gehrels Swift X-ray Observatory (hereafter Swift; N. Gehrels et al. 2004) and Konus-Wind (hereafter Konus; R. L. Aptekar et al. 1995) or Swift and the Fermi Gamma-Ray Burst Monitor (hereafter GBM; C. Meegan et al. 2009). It includes apparently energetic GRBs from the catalogs of A. Tsvetkova et al. (2017), A. Tsvetkova et al. (2021), and S. Poolakkil et al. (2021), in this order.

We start with the catalogs of A. Tsvetkova et al. (2017, 2021), which are mutually exclusive and, respectively, contain 84 and 42 apparently energetic GRBs, and complete the sample with 26 apparently energetic GRBs listed in S. Poolakkil et al. (2021), which are not in the Konus catalogs. We use the measurements of $E_{\rm iso}$ provided in these catalogs without recalculating them, considering that the instrument teams are the best placed to compute this parameter from the data recorded by their instrument. These three catalogs use the same cosmological parameters (Planck Collaboration et al. 2014), allowing for the direct comparison of $E_{\rm iso}$.

Finally, the sample is completed with 33 apparently energetic GRBs detected up to the end of 2023, which occurred after the publication of the previous catalogs, including the Brightest Of All Time (BOAT) GRB 221009A, whose prompt emission has been measured by several instruments (Z.-H. An et al. 2023; E. Burns et al. 2023; D. Frederiks et al. 2023b; J. Řípa et al. 2023; L. J. Mitchell et al. 2025; V. Savchenko et al. 2024). This sample more than doubles the number of apparently energetic GRBs presented in A17, which included 75 GRBs with $E_{\rm iso} \geqslant 10^{53}$ erg.

These bursts are listed in Table 1, which gives their name, redshift, and $E_{\rm iso}$ with its error. A graphical view of this sample is shown in Figure 1, which displays $E_{\rm iso}$ as a function of the comoving volume enclosed within the redshift of the GRB. This plot emphasizes the very special position of GRB 221009A, which is at the same time the closest and the apparently most energetic burst in our sample, as emphasized by various authors (Z.-H. An et al. 2023; E. Burns et al. 2023; D. Frederiks et al. 2023b; L. Lan et al. 2023; T. Laskar et al. 2023; J. Řípa et al. 2023; M. Tavani et al. 2023; M. A. Williams et al. 2023). Figure 1 additionally shows that our sample is not strongly affected by selection biases since apparently energetic GRBs, with $E_{\rm iso} \sim 10^{53}$ erg, are detected up to the largest distances.

3. Fitting the Bright End of the $E_{\rm iso}$ Distribution

In order to verify the existence of the energy cutoff discussed in A17, A. Tsvetkova et al. (2017) and L. Lan et al. (2023), we fitted the differential energy distribution above 10^{53} erg with a simple power law (PL), a cutoff power law (CPL), or a broken power law (BPL). We fitted two samples: the 185 GRBs in Table 1, including the BOAT, and the same sample without the BOAT. Regarding the BOAT, various authors have measured different values of its isotropic equivalent energy $E_{\rm iso}$ (see the references in Table 1), and we have chosen the measurement of the Konus team ($E_{\rm iso} = 1.2 \times 10^{55}$ erg; D. Frederiks et al. 2023b) for consistency with the majority of the measurements in Table 1, which also come from Konus. This is also an intermediate value between Fermi ($E_{\rm iso} = 1.0 \times 10^{55}$ erg; S. Lesage et al. 2023) and GECAM ($E_{\rm iso} = 1.5 \times 10^{55}$ erg; Z.-H. An et al. 2023). We have checked that this choice impacts only marginally the numbers in Table 2 (at most a few %).

For each function (PL, CPL, BPL), the best-fit parameters are those that maximize the log-likelihood of the observed differential $E_{\rm iso}$ distribution. To determine the confidence intervals on the parameters, we use the classical approximation of the quantity $-2 \times [\ln L(x_i, \theta) - \ln L(x_i, \hat{\theta})]$ by a chi-square distribution with ν degrees of freedom, where ν is the number of parameters of the fitting function. Here, $\ln L(x_i, \hat{\theta})$ is the log-likelihood of the sample for the best-fit parameters, and $\ln L(x_i, \theta)$ is the log-likelihood of the same sample for an arbitrary value of θ. After a verification that the statistical uncertainties dominate over the contribution of the uncertainties on $E_{\rm iso}$, we provide the best-fit parameters and their errors computed with this procedure in Table 2.

These fits can be used to test the existence of the cutoff. A Kolmogorov–Smirnov (KS) test shows that the addition of a cutoff around 4×10^{54} erg increases the probability of the fits from about 1% to about 50%. The Bayesian information criterion (BIC; G. Schwarz 1978) is often used to compare two fits of the same sample. The BIC is given by $\mathrm{BIC} = -2\ln(L) + k\ln(N)$, where k is the number of fit parameters, N is the number of points in the sample, and L is the maximum likelihood of the sample. Adding a parameter improves the fit, increases the likelihood, and usually reduces the BIC. The BIC reduction offers a way to measure the improvement brought by the supplementary parameter. The addition of a parameter is usually considered statistically justified if the BIC reduction exceeds 6. With respect to the PL fit, both the CPL and the BPL lead to significant reductions of the BIC (16 and 17, respectively), fully justifying the addition of the cutoff from a statistical perspective. The BIC, however, does not suggest a preferred model between CPL and BPL, from statistical grounds only. Finally, we note that including the BOAT changes the values of the parameters slightly, without removing the need for a cutoff.

Table 2 also indicates, for each distribution, the probability of getting a GRB as apparently energetic as GRB 221009A. For the best-fit CPL distribution, this probability is of the order of 0.1%. Considering only the shape of the apparent energy distribution, it is thus not surprising to observe one GRB as apparently energetic as GRB 221009A in a sample of nearly 200 apparently energetic GRBs: GRB 221009A appears as an extreme event, but not as a clear outlier to this distribution. This conclusion, however, does not take the proximity of the BOAT into account, a point which is discussed in Section 4.1.

The cumulative best-fit PL, CPL, and BPL functions are shown in Figure 2, on top of the observed cumulative $E_{\rm iso}$ distribution (note that the slope of the cumulative distribution is obtained by adding 1 to the numbers in Table 2). This figure clearly shows the fast decrease in the number of apparently energetic GRBs beyond a few times 10^{54} erg.

Table 1
184 GRBs Used in This Study

GRB Name	Redshift	Eiso (10^{52} erg)	Satellite	References
GRB 970828	0.96	$26.2^{+0.9}_{-0.9}$	KONUS	A. Tsvetkova et al. (2017)
GRB 971214	3.42	$14.6^{+0.6}_{-0.6}$	KONUS	A. Tsvetkova et al. (2017)
GRB 990123	1.60	$213.3^{+5.4}_{-5.4}$	KONUS	A. Tsvetkova et al. (2017)
GRB 990506	1.31	$125.5^{+4.3}_{-4.3}$	KONUS	A. Tsvetkova et al. (2017)
GRB 990510	1.62	$17.4^{+0.8}_{-0.8}$	KONUS	A. Tsvetkova et al. (2017)
GRB 990705	0.84	$21.8^{+0.8}_{-0.8}$	KONUS	A. Tsvetkova et al. (2017)
GRB 991208	0.71	$23.3^{+0.5}_{-0.5}$	KONUS	A. Tsvetkova et al. (2017)
GRB 991216	1.02	$88.6^{+1.1}_{-1.1}$	KONUS	A. Tsvetkova et al. (2017)
GRB 000131	4.50	$181.7^{+5.6}_{-5.6}$	KONUS	A. Tsvetkova et al. (2017)
GRB 000210	0.85	$19.3^{+0.5}_{-0.5}$	KONUS	A. Tsvetkova et al. (2017)
GRB 000911	1.06	$64.9^{+2.0}_{-2.0}$	KONUS	A. Tsvetkova et al. (2017)
GRB 000926	2.04	$27.8^{+1.1}_{-1.1}$	KONUS	A. Tsvetkova et al. (2017)
GRB 010222	1.48	$107.2^{+3.0}_{-3.0}$	KONUS	A. Tsvetkova et al. (2017)
GRB 020124	3.198	$21.9^{+3.1}_{-2.8}$	HET	J. Hjorth et al. (2003), J. L. Atteia et al. (2005)
GRB 020405	0.69	$11.7^{+0.2}_{-0.2}$	KONUS	A. Tsvetkova et al. (2017)
GRB 020813	1.25	$75.8^{+4.7}_{-4.7}$	KONUS	A. Tsvetkova et al. (2017)
GRB 030328	1.5216	$37.9^{+1.4}_{-1.4}$	HET	E. Maiorano et al. (2006), T. Sakamoto et al. (2005)
GRB 050401	2.90	$46.4^{+2.2}_{-2.2}$	KONUS	A. Tsvetkova et al. (2017)
GRB 050505	4.27	$19.2^{+2.7}_{-2.2}$	KONUS	A. Tsvetkova et al. (2021)
GRB 050730	3.9693	$68.6^{+32.5}_{-25.5}$	KONUS	A. Tsvetkova et al. (2021)
GRB 050814	5.77	$12.2^{+4.0}_{-3.6}$	KW1	P. A. Curran et al. (2008), A. Tsvetkova et al. (2021)
GRB 050820A	2.61	$103.6^{+3.6}_{-3.6}$	KONUS	A. Tsvetkova et al. (2017)
GRB 050904	6.295	$147.7^{+20.4}_{-18.8}$	KONUS	A. Tsvetkova et al. (2021)
GRB 050922C	2.20	$10.2^{+2.4}_{-2.4}$	KONUS	A. Tsvetkova et al. (2017)
GRB 051008	2.77	$83.4^{+7.0}_{-7.0}$	KONUS	A. Tsvetkova et al. (2017)
GRB 051022	0.81	$49.0^{+1.0}_{-1.0}$	KONUS	A. Tsvetkova et al. (2017)
GRB 060124	2.30	$32.8^{+1.5}_{-1.5}$	KONUS	A. Tsvetkova et al. (2017)
GRB 060210	3.9122	$112.7^{+13.4}_{-14.4}$	KONUS	A. Tsvetkova et al. (2021)
GRB 060418	1.4901	$14.7^{+0.9}_{-0.9}$	KONUS	A. Tsvetkova et al. (2021)
GRB 060607A	3.0749	$16.3^{+1.9}_{-1.6}$	KONUS	A. Tsvetkova et al. (2021)
GRB 060714	2.7108	$10.5^{+3.2}_{-1.6}$	KONUS	A. Tsvetkova et al. (2021)
GRB 060814	1.9200	$41.4^{+2.5}_{-2.5}$	KONUS	A. Tsvetkova et al. (2017)
GRB 060906	3.6856	$19.3^{+2.1}_{-1.8}$	KONUS	A. Tsvetkova et al. (2021)
GRB 060927	5.4636	$22.6^{+3.0}_{-2.8}$	KONUS	A. Tsvetkova et al. (2021)
GRB 061007	1.26	$111.3^{+4.0}_{-4.0}$	KONUS	A. Tsvetkova et al. (2017)
GRB 061121	1.31	$30.4^{+1.1}_{-1.1}$	KONUS	A. Tsvetkova et al. (2017)
GRB 061222A	2.09	$26.0^{+0.7}_{-0.7}$	KONUS	A. Tsvetkova et al. (2017)
GRB 070125	1.55	$127.8^{+6.4}_{-6.4}$	KONUS	A. Tsvetkova et al. (2017)
GRB 070328	2.06	$77.7^{+8.5}_{-8.5}$	KONUS	A. Tsvetkova et al. (2017)
GRB 070411	2.9538	$15.6^{+4.7}_{-3.4}$	KONUS	A. Tsvetkova et al. (2021)
GRB 070419B	1.9588	$27.4^{+3.0}_{-2.8}$	KONUS	A. Tsvetkova et al. (2021)
GRB 070521	2.0865	$21.1^{+0.6}_{-0.7}$	KW1	T. Krühler et al. (2015), A. Tsvetkova et al. (2017)
GRB 070721B	3.6298	$27.0^{+11.7}_{-8.3}$	KONUS	A. Tsvetkova et al. (2021)
GRB 071003	1.60	$38.5^{+1.8}_{-1.8}$	KONUS	A. Tsvetkova et al. (2017)
GRB 071025	5.2	$76.7^{+7.5}_{-6.1}$	KONUS	A. Tsvetkova et al. (2021)
GRB 080207	2.0858	$16.1^{+2.4}_{-1.8}$	KONUS	A. Tsvetkova et al. (2021)
GRB 080319B	0.94	$156.7^{+1.9}_{-1.9}$	KONUS	A. Tsvetkova et al. (2017)
GRB 080319C	1.95	$15.5^{+1.6}_{-1.6}$	KONUS	A. Tsvetkova et al. (2017)
GRB 080411	1.03	$23.9^{+0.8}_{-0.8}$	KONUS	A. Tsvetkova et al. (2017)
GRB 080603B	2.69	$10.0^{+1.7}_{-1.7}$	KONUS	A. Tsvetkova et al. (2017)
GRB 080605	1.64	$24.0^{+0.5}_{-0.5}$	KONUS	A. Tsvetkova et al. (2017)
GRB 080607	3.04	$217.1^{+6.0}_{-6.0}$	KONUS	A. Tsvetkova et al. (2017)
GRB 080721	2.59	$150.9^{+6.3}_{-6.3}$	KONUS	A. Tsvetkova et al. (2017)
GRB 080804	2.2045	$14.3^{+0.6}_{-0.6}$	FERMI	S. Poolakkil et al. (2021)
GRB 080810	3.35	$47.9^{+1.6}_{-1.6}$	FERMI	S. Poolakkil et al. (2021)
GRB 080906	2.13	$18.3^{+3.0}_{-2.8}$	KONUS	A. Tsvetkova et al. (2021)
GRB 080916C	4.35	$482.0^{+39.0}_{-39.0}$	KONUS	A. Tsvetkova et al. (2017)

Table 1
(Continued)

GRB Name	Redshift	Eiso (10^{52} erg)	Satellite	References
GRB 081008	1.9685	$14.4^{+3.0}_{-2.5}$	KONUS	A. Tsvetkova et al. (2021)
GRB 081028A	3.038	$20.0^{+3.1}_{-2.1}$	KONUS	A. Tsvetkova et al. (2021)
GRB 081029	3.8479	$20.5^{+8.5}_{-5.1}$	KONUS	A. Tsvetkova et al. (2021)
GRB 081121	2.51	$23.5^{+1.0}_{-1.0}$	KONUS	A. Tsvetkova et al. (2017)
GRB 081203A	2.05	$28.5^{+9.6}_{-9.6}$	KONUS	A. Tsvetkova et al. (2017)
GRB 081221	2.26	$39.7^{+1.0}_{-1.0}$	KONUS	A. Tsvetkova et al. (2017)
GRB 081222	2.77	$17.8^{+1.2}_{-1.2}$	KONUS	A. Tsvetkova et al. (2017)
GRB 090102	1.55	$20.0^{+1.0}_{-1.0}$	KONUS	A. Tsvetkova et al. (2017)
GRB 090201	2.10	$95.5^{+2.8}_{-2.8}$	KONUS	A. Tsvetkova et al. (2017)
GRB 090323	3.60	$581.0^{+44.0}_{-44.0}$	KONUS	A. Tsvetkova et al. (2017)
GRB 090328	0.74	$10.9^{+0.8}_{-0.8}$	KONUS	A. Tsvetkova et al. (2017)
GRB 090418A	1.608	$14.2^{+1.2}_{-1.1}$	KONUS	A. Tsvetkova et al. (2021)
GRB 090429B	9.38	$10.2^{+2.7}_{-2.3}$	KONUS	A. Tsvetkova et al. (2021)
GRB 090516	4.109	$104.0^{+4.0}_{-4.0}$	FERMI	S. Poolakkil et al. (2021)
GRB 090519	3.85	$25.7^{+1.6}_{-1.6}$	FERMI	S. Poolakkil et al. (2021)
GRB 090618	0.54	$25.3^{+0.5}_{-0.5}$	KONUS	A. Tsvetkova et al. (2017)
GRB 090715B	3.00	$20.5^{+1.9}_{-1.9}$	KONUS	A. Tsvetkova et al. (2017)
GRB 090812	2.45	$27.2^{+1.0}_{-1.0}$	KONUS	A. Tsvetkova et al. (2017)
GRB 090902B	1.822	$402.0^{+1.2}_{-1.2}$	FERMI	S. Poolakkil et al. (2021)
GRB 090926A	2.11	$211.1^{+5.3}_{-5.3}$	KONUS	A. Tsvetkova et al. (2017)
GRB 091003	0.8969	$10.2^{+0.2}_{-0.2}$	FERMI	S. Poolakkil et al. (2021)
GRB 091029	2.752	$15.7^{+2.4}_{-2.5}$	KONUS	A. Tsvetkova et al. (2021)
GRB 100414A	1.37	$53.5^{+1.1}_{-1.1}$	KONUS	A. Tsvetkova et al. (2017)
GRB 100606A	1.55	$29.4^{+2.3}_{-2.3}$	KONUS	A. Tsvetkova et al. (2017)
GRB 100724A	1.288	$146.0^{+0.8}_{-0.8}$	FERMI	S. Poolakkil et al. (2021)
GRB 100728A	1.57	$114.0^{+6.8}_{-6.8}$	KONUS	A. Tsvetkova et al. (2017)
GRB 100906A	1.73	$24.9^{+2.7}_{-2.7}$	KONUS	A. Tsvetkova et al. (2017)
GRB 110205A	2.22	$63.0^{+4.9}_{-4.5}$	KONUS	A. Tsvetkova et al. (2021)
GRB 110422A	1.77	$74.7^{+1.1}_{-1.1}$	KONUS	A. Tsvetkova et al. (2017)
GRB 110503A	1.61	$21.3^{+1.0}_{-1.0}$	KONUS	A. Tsvetkova et al. (2017)
GRB 110731A	2.83	$31.5^{+1.2}_{-1.2}$	KONUS	A. Tsvetkova et al. (2017)
GRB 110818A	3.36	$19.2^{+1.3}_{-1.3}$	FERMI	S. Poolakkil et al. (2021)
GRB 110918A	0.98	$270.5^{+9.9}_{-9.9}$	KONUS	A. Tsvetkova et al. (2017)
GRB 111008A	5.00	$41.4^{+7.1}_{-7.1}$	KONUS	A. Tsvetkova et al. (2017)
GRB 111123A	3.1516	$39.0^{+4.7}_{-3.8}$	KONUS	A. Tsvetkova et al. (2021)
GRB 120119A	1.73	$40.2^{+2.8}_{-2.8}$	KONUS	A. Tsvetkova et al. (2017)
GRB 120327A	2.813	$19.1^{+1.9}_{-1.6}$	KONUS	A. Tsvetkova et al. (2021)
GRB 120404A	2.876	$10.3^{+1.8}_{-1.4}$	KONUS	A. Tsvetkova et al. (2021)
GRB 120521C	6.	$19.5^{+4.9}_{-3.6}$	KONUS	A. Tsvetkova et al. (2021)
GRB 120624B	2.20	$282.0^{+12.0}_{-12.0}$	KONUS	A. Tsvetkova et al. (2017)
GRB 120711A	1.41	$203.7^{+4.6}_{-4.6}$	KONUS	A. Tsvetkova et al. (2017)
GRB 120712A	4.1745	$17.5^{+1.0}_{-1.0}$	FERMI	S. Poolakkil et al. (2021)
GRB 120716A	2.49	$26.4^{+2.5}_{-2.5}$	KONUS	A. Tsvetkova et al. (2017)
GRB 120802A	3.796	$13.1^{+1.7}_{-1.7}$	KONUS	A. Tsvetkova et al. (2021)
GRB 120909A	3.93	$65.3^{+2.6}_{-2.6}$	FERMI	S. Poolakkil et al. (2021)
GRB 120922A	3.1	$44.6^{+1.8}_{-1.8}$	FERMI	S. Poolakkil et al. (2021)
GRB 121128A	2.20	$10.1^{+0.4}_{-0.4}$	KONUS	A. Tsvetkova et al. (2017)
GRB 130408A	3.76	$32.4^{+6.1}_{-6.1}$	KONUS	A. Tsvetkova et al. (2017)
GRB 130427A	0.34	$89.0^{+0.5}_{-0.5}$	KONUS	A. Tsvetkova et al. (2017)
GRB 130505A	2.27	$438.0^{+10.0}_{-10.0}$	KONUS	A. Tsvetkova et al. (2017)
GRB 130514A	3.6	$61.5^{+6.1}_{-5.1}$	KONUS	A. Tsvetkova et al. (2021)
GRB 130518A	2.49	$216.0^{+14.0}_{-14.0}$	KONUS	A. Tsvetkova et al. (2017)
GRB 130606A	5.91	$85.1^{+20.7}_{-21.1}$	KONUS	A. Tsvetkova et al. (2021)
GRB 130907A	1.24	$384.0^{+13.0}_{-13.0}$	KONUS	A. Tsvetkova et al. (2017)
GRB 131011A	1.874	$11.8^{+0.5}_{-0.5}$	FERMI	S. Poolakkil et al. (2021)
GRB 131030A	1.29	$32.7^{+1.3}_{-1.3}$	KONUS	A. Tsvetkova et al. (2017)
GRB 131105A	1.69	$15.3^{+1.2}_{-1.2}$	KONUS	A. Tsvetkova et al. (2017)

Table 1
(Continued)

GRB Name	Redshift	Eiso (10^{52} erg)	Satellite	References
GRB 131108A	2.40	$54.0^{+2.4}_{-2.4}$	KONUS	A. Tsvetkova et al. (2017)
GRB 131231A	0.64	$21.1^{+0.6}_{-0.6}$	KONUS	A. Tsvetkova et al. (2017)
GRB 140114A	3.0	$16.0^{+2.7}_{-2.1}$	KONUS	A. Tsvetkova et al. (2021)
GRB 140206A	2.73	$25.0^{+0.5}_{-0.5}$	FERMI	S. Poolakkil et al. (2021)
GRB 140213A	1.2076	$10.6^{+0.1}_{-0.1}$	FERMI	S. Poolakkil et al. (2021)
GRB 140304A	5.283	$11.2^{+0.9}_{-0.9}$	FERMI	S. Poolakkil et al. (2021)
GRB 140311A	4.954	$25.9^{+7.7}_{-5.6}$	KONUS	A. Tsvetkova et al. (2021)
GRB 140419A	3.96	$228.0^{+18.0}_{-18.0}$	KONUS	A. Tsvetkova et al. (2017)
GRB 140423A	3.26	$50.3^{+2.0}_{-2.0}$	FERMI	S. Poolakkil et al. (2021)
GRB 140508A	1.03	$22.5^{+1.5}_{-1.5}$	KONUS	A. Tsvetkova et al. (2017)
GRB 140512A	0.725	$10.0^{+0.2}_{-0.2}$	FERMI	S. Poolakkil et al. (2021)
GRB 140614A	4.233	$17.5^{+4.6}_{-6.4}$	KONUS	A. Tsvetkova et al. (2021)
GRB 140703A	3.14	$24.4^{+1.1}_{-1.1}$	FERMI	S. Poolakkil et al. (2021)
GRB 141028A	2.33	$67.5^{+0.9}_{-0.9}$	FERMI	S. Poolakkil et al. (2021)
GRB 141109A	2.993	$39.5^{+3.8}_{-3.2}$	KONUS	A. Tsvetkova et al. (2021)
GRB 150206A	2.09	$61.9^{+4.5}_{-4.5}$	KONUS	A. Tsvetkova et al. (2017)
GRB 150314A	1.76	$76.8^{+2.1}_{-2.1}$	KONUS	A. Tsvetkova et al. (2017)
GRB 150403A	2.06	$116.4^{+6.2}_{-6.2}$	KONUS	A. Tsvetkova et al. (2017)
GRB 150413A	3.139	$40.8^{+7.2}_{-7.5}$	KONUS	A. Tsvetkova et al. (2021)
GRB 150821A	0.76	$15.5^{+1.2}_{-1.2}$	KONUS	A. Tsvetkova et al. (2017)
GRB 151021A	2.33	$112.7^{+9.4}_{-9.4}$	KONUS	A. Tsvetkova et al. (2017)
GRB 151111A	3.5	$13.8^{+1.8}_{-1.6}$	KONUS	A. Tsvetkova et al. (2021)
GRB 160131A	0.97	$87.0^{+6.6}_{-6.6}$	KONUS	A. Tsvetkova et al. (2017)
GRB 160227A	2.38	$25.3^{+6.3}_{-5.8}$	KONUS	A. Tsvetkova et al. (2021)
GRB 160327A	4.99	$20.8^{+4.9}_{-4.7}$	KONUS	A. Tsvetkova et al. (2021)
GRB 160509A	1.17	$113.0^{+10.0}_{-10.0}$	KONUS	A. Tsvetkova et al. (2017)
GRB 160623A	0.37	$25.3^{+0.3}_{-0.3}$	KONUS	A. Tsvetkova et al. (2017)
GRB 160625B	1.41	$510.1^{+6.2}_{-6.2}$	KONUS	A. Tsvetkova et al. (2017)
GRB 160629A	3.33	$38.9^{+1.4}_{-1.4}$	KONUS	A. Tsvetkova et al. (2017)
GRB 161014A	2.823	$10.7^{+0.5}_{-0.5}$	FERMI	S. Poolakkil et al. (2021)
GRB 161017A	2.013	$16.5^{+4.2}_{-3.2}$	KONUS	A. Tsvetkova et al. (2021)
GRB 161023A	2.7106	$69.5^{+9.9}_{-9.9}$	KW1	A. de Ugarte Postigo et al. (2018), D. Frederiks et al. (2016)
GRB 161117A	1.549	$23.6^{+0.3}_{-0.3}$	FERMI	S. Poolakkil et al. (2021)
GRB 170202A	3.645	$22.7^{+3.7}_{-3.1}$	KONUS	A. Tsvetkova et al. (2021)
GRB 170214A	2.53	$414.0^{+2.3}_{-2.3}$	FERMI	S. Poolakkil et al. (2021)
GRB 170405A	3.51	$252.0^{+2.9}_{-2.9}$	FERMI	S. Poolakkil et al. (2021)
GRB 170705A	2.01	$12.5^{+0.4}_{-0.4}$	FERMI	S. Poolakkil et al. (2021)
GRB 171010A	0.3285	$22.1^{+0.1}_{-0.1}$	FERMI	S. Poolakkil et al. (2021)
GRB 180314A	1.445	$10.4^{+0.2}_{-0.2}$	FERMI	S. Poolakkil et al. (2021)
GRB 180325A	2.248	$22.3^{+3.6}_{-3.5}$	KW1	P. D'Avanzo et al. (2018a); D. Frederiks et al. (2018a)
GRB 180624A	2.855	$19.4^{+4.7}_{-3.6}$	KONUS	A. Tsvetkova et al. (2021)
GRB 180720B	0.654	$60.1^{+2.9}_{-2.8}$	KW1	P. M. Vreeswijk et al. (2018), D. Frederiks et al. (2018b)
GRB 180914B	1.096	$336.9^{+14.6}_{-14.7}$	KW1	P. D'Avanzo et al. (2018b), D. Frederiks et al. (2018c)
GRB 181020A	2.938	$69.6^{+9.7}_{-9.0}$	KW1	J. P. U. Fynbo et al. (2018), A. Tsvetkova et al. (2018)
GRB 181110A	1.505	$20.7^{+3.7}_{-2.6}$	KONUS	A. Tsvetkova et al. (2021)
GRB 181201A	0.45	$12.8^{+0.4}_{-0.4}$	KW1	L. Izzo et al. (2018), D. Svinkin et al. (2018)
GRB 190106A	1.859	$11.2^{+2.5}_{-1.7}$	KW1	P. Schady et al. (2019), A. Tsvetkova et al. (2019)
GRB 190114C	0.4245	$21.5^{+0.3}_{-0.3}$	KW1	A. J. Castro-Tirado et al. (2019), A. Ursi et al. (2020)
GRB 190530A	0.9386	$134.4^{+3.7}_{-3.6}$	KW1	R. Gupta et al. (2022), D. Frederiks et al. (2019a)
GRB 191004B	3.5055	$11.4^{+1.2}_{-1.1}$	KW1	J. B. Vielfaure et al. (2020b), D. Svinkin et al. (2019)
GRB 191221B	1.148	$34.8^{+3.5}_{-3.5}$	KW1	J. B. Vielfaure et al. (2019), D. Frederiks et al. (2019b)
GRB 200524A	1.256	$13.7^{+2.9}_{-2.5}$	KW1	Y. Yao et al. (2021), D. Svinkin et al. (2020a)
GRB 200613A	1.2255	$20.3^{+0.2}_{-0.3}$	FER	A. de Ugarte Postigo et al. (2021a), E. Bissaldi et al. (2020)
GRB 200829A	1.29	$126.0^{+2.9}_{-3.0}$	KW1	N. S. Pankov et al. (2023), A. Ridnaia et al. (2020)
GRB 201103B	1.105	$17.0^{+2.7}_{-2.5}$	KW1	D. Xu et al. (2020), D. Svinkin et al. (2020b)
GRB 201216C	1.10	$60.6^{+3.3}_{-3.3}$	KW1	J. B. Vielfaure et al. (2020a), D. Frederiks et al. (2020a)
GRB 201221A	5.70	$25.1^{+10.9}_{-4.7}$	KW1	D. B. Malesani et al. (2020), D. Frederiks et al. (2020b)

Table 1
(Continued)

GRB Name	Redshift	Eiso (10^{52} erg)	Satellite	References
GRB 210610B	1.1345	$46.2^{+3.6}_{-3.5}$	KW1	A. de Ugarte Postigo et al. (2021c), D. Frederiks et al. (2021a)
GRB 210619B	1.937	$385.2^{+10.9}_{-10.9}$	KW1	A. de Ugarte Postigo et al. (2021b), D. Svinkin et al. (2021)
GRB 210702A	1.16	$77.1^{+6.1}_{-6.2}$	KW1	D. Xu et al. (2021), D. Frederiks et al. (2021b)
GRB 210822A	1.736	$85.3^{+7.8}_{-7.8}$	KW1	Z. P. Zhu et al. (2021), D. Frederiks et al. (2021c)
GRB 210905A	6.318	$127.0^{+20.0}_{-19.0}$	KW1	N. Tanvir et al. (2021), A. Rossi et al. (2022)
GRB 220101A	4.618	$324.0^{+21.0}_{-20.0}$	KW1	J. P. U. Fynbo et al. (2022), A. Tsvetkova et al. (2022); A. Tsvetkova & KW Team (2022)
GRB 220107A	1.246	$23.9^{+1.5}_{-1.3}$	KW1	A. J. Castro-Tirado et al. (2022), A. Ridnaia et al. (2022)
GRB 220117A	4.961	$15.3^{+3.8}_{-3.8}$	KW1	J. Palmerio et al. (2022), D. Frederiks et al. (2022b)
GRB 220527A	0.857	$12.8^{+0.6}_{-0.7}$	KW1	D. Xu et al. (2022), A. Lysenko et al. (2022)
GRB 220627A	3.084	$244.0^{+28.0}_{-27.0}$	KW1	L. Izzo et al. (2022), D. Frederiks et al. (2022a)
GRB 230204B	2.142	$227.0^{+3.0}_{-2.0}$	FER	A. Saccardi et al. (2023), S. Poolakkil et al. (2023)
GRB 230812B	0.360	$11.5^{+0.2}_{-0.3}$	KW1	A. de Ugarte Postigo et al. (2023), D. Frederiks et al. (2023a)
GRB 231215A	2.305	$114.0^{+11.0}_{-10.0}$	KW1	C. C. Thoene et al. (2023), D. Frederiks et al. (2023b)
GRB 221009A	0.151	280^{+80}_{-50}	ALPHA	J. Řípa et al. (2023)
		740^{+10}_{-10}	SIRI	L. J. Mitchell et al. (2025)
		1500^{+20}_{-16}	GECAM-C	Z.-H. An et al. (2023)
		1010^{+7}_{-7}	FERMI	S. Lesage et al. (2023)
		1200^{+100}_{-100}	KONUS	D. Frederiks et al. (2023b)

(This table is available in machine-readable form in the online article.)

3.1. Comparison with the Work of L. Lan et al. (2023)

In a similar work, L. Lan et al. (2023) studied the energy distribution of 355 GRBs with $E_{\rm iso} \geqslant 10^{52}$ erg (319 long and 36 short), and compared GRB 221009A with apparently very energetic GRBs with $E_{\rm iso} \geqslant 10^{54}$ erg. The number of GRBs with $E_{\rm iso} \geqslant 10^{53}$ erg in their study (158 GRBs) is comparable to this work (185 GRBs).

They too conclude that a cutoff PL or a BPL law is strongly preferred over a simple power law. It is not possible to directly compare the parameters in their study with ours, because they fit the cumulative energy distribution of GRBs with $E_{\rm iso} \geqslant 10^{52}$ erg, while we work with the unbinned differential energy distribution of GRBs with $E_{\rm iso} \geqslant 10^{53}$ erg. In order to perform a relevant comparison, we have (i) used their sample to calculate the best-fit parameters for a CPL function fitting the cumulative energy distribution of GRBs with $E_{\rm iso} \geqslant 10^{52}$ erg, and (ii) restricted their sample to GRBs with $E_{\rm iso} \geqslant 10^{53}$ erg to calculate the best-fit parameters for a CPL function fitting the differential energy distribution (see Figure 3 for this comparison). In both cases we find values compatible with theirs, showing the consistency of our analyses.

4. Discussion

4.1. The Case of GRB 221009A

Figure 1 clearly shows that GRB 221009A was a remarkable GRB, combining the shortest distance (by far) and the highest $E_{\rm iso}$ in our sample. We evaluate below the probability for GRB 221009A to be randomly drawn from of our sample.

What is the probability of observing a GRB closer than $z = 0.151$? The sample contains 184 GRBs up to redshift $z = 6.3$ (excluding GRB 090429B at $z = 9.38$, which is the only burst in our sample detected beyond $z = 6.3$, where the identification of the afterglow requires near-infrared observations). Considering the density evolution proposed by J. Palmerio et al. (2022), GRBs closer than $z = 0.151$ represent a fraction $p_2 = 4.3 \times 10^{-4}$ of the number of GRBs within $z = 6.3$. The chance to have 1 GRB closer than $z = 0.151$ among 184 events in our sample is thus $p = 1 - (1 - p_2)^{184} \approx 0.08$.

This calculation does not take into account, however, the fact that GRB 221009A has also the highest $E_{\rm iso}$. If one assumes the absence of luminosity or energy evolution with redshift, the probability of GRB 221009A in our sample is simply given by: $p = 1 - (1 - p_1 \times p_2)^{184} = 1.4 \times 10^{-4}$ (where $p_1 = 1.7 \times 10^{-3}$ is given in Table 2). While our ignorance of the joint $E_{\rm iso}$–redshift distribution prevents us from computing reliably the probability that the most apparently energetic GRB observed so far is also the closest, it is clear that the observation of a GRB as close and as apparently energetic as GRB 221009A is truly exceptional. This unique combination of distance and $E_{\rm iso}$ explains the outstanding brightness of GRB 221009A. The rarity of GRB 221009A is confirmed by various authors, who evaluate the rate of such events from 1 per 10^2–10^4 yr (E. Burns et al. 2023; D. B. Malesani et al. 2023; B. O'Connor et al. 2023; M. A. Williams et al. 2023).

Apart from its extreme isotropic energy, GRB 221009A seems to possess most characteristics of classical LGRBs, with respect to its prompt emission (Z.-H. An et al. 2023; E. Burns et al. 2023; D. Frederiks et al. 2023b; D. A. Kann et al. 2023; S. Lesage et al. 2023; J. Řípa et al. 2023; M. Tavani et al. 2023; V. Savchenko et al. 2024), to its afterglow (M. D. Fulton et al. 2023; T. Laskar et al. 2023; LHAASO Collaboration et al. 2023; M. A. Williams et al. 2023), and to its association with a broad-line supernova (M. D. Fulton et al. 2023; M. Shrestha et al. 2023; G. P. Srinivasaragavan et al. 2023; P. K. Blanchard et al. 2024; D.-F. Kong et al. 2024). The afterglow modeling indicates a narrow jet, with an opening angle in the range of 0.6°–2° (Z.-H. An et al. 2023; J. S. Bright et al. 2023; Z. Cao et al. 2023; Y. Sato et al. 2023). This narrow jet strongly reduces the energy budget of the jet, bringing it in the range

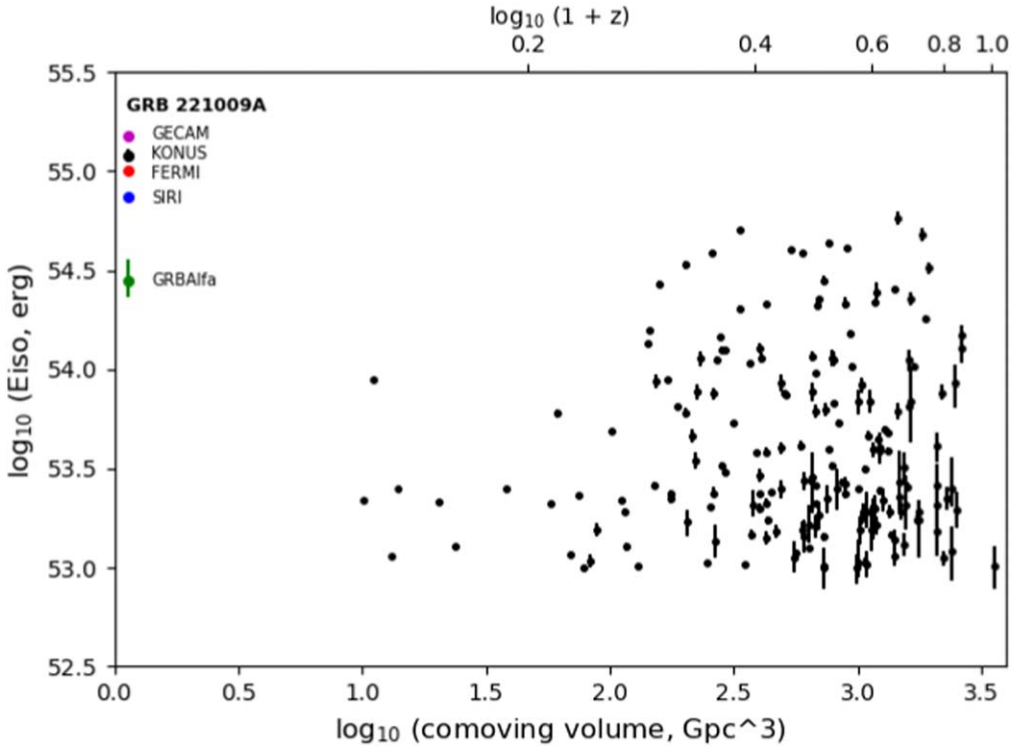

Figure 1. Distribution of 185 apparently energetic GRBs showing their isotropic equivalent energy E_{iso} and its uncertainty as a function of the volume enclosed within their distance. The colored points show the position of GRB 221009A, based on the isotropic equivalent energy measured by GRBAlpha (J. Řípa et al. 2023, green), SIRI-2 (L. J. Mitchell et al. 2025, blue), Fermi (S. Lesage et al. 2022, red), Konus (D. Frederiks et al. 2023b, black), GECAM (Z.-H. An et al. 2023, magenta). For a large fraction of the sample, the error bars on E_{iso} are smaller than the symbol, including the SIRI, Fermi, and GECAM measurements of GRB 221009A. This figure emphasizes the peculiar location of GRB 221009A, which is both the closest of apparently energetic GRBs and the apparently most energetic of them.

Table 2
Best-fit Parameters of the Slope of the Differential E_{iso} Distribution, for the PL, CPL, and BPL Models

Fit	Sample	Slope 1	E_{break} (10^{54} erg)	Slope 2	KS test probability	$P(E_{iso} > 1.2 \times 10^{55})$ (p_1)	BIC reduction
PL	184 GRBs	-1.71 ± 0.05	⋯	⋯	0.011	3.3×10^{-2}	N/A
	184 GRBs + BOAT	-1.70 ± 0.05	⋯	⋯	0.013	3.4×10^{-2}	N/A
CPL	184 GRBs	-1.26 ± 0.18	$3.2^{+2.6}_{-1.1}$	⋯	0.45	7.0×10^{-4}	19.5
	184 GRBs + BOAT	-1.32 ± 0.17	$4.2^{+3.9}_{-1.5}$	⋯	0.55	1.7×10^{-3}	16.3
BPL	184 GRBs	-1.48 ± 0.13	$5.0^{+1.4}_{-1.5}$	$\leqslant -3.6$	0.51	3.5×10^{-6}	23.7
	184 GRBs + BOAT	-1.48 ± 0.14	$4.0^{+2.3}_{-2.0}$	$-4.0^{+1.6}_{-4.0}$	0.50	1.2×10^{-3}	17.4

Note. The KS test probability and the BIC reduction measure the statistical justification of the cutoff (see text).

7×10^{50}–7×10^{51} erg in gamma rays, in agreement with classical GRBs (D. A. Frail et al. 2001). Finally, the theoretical modeling also supports the interpretation of GRB 221009A as a classical LGRB with a structured jet with a very narrow core (B. O'Connor et al. 2023; J. Ren et al. 2023; Y. Sato et al. 2023; J. Yang et al. 2023; B. T. Zhang et al. 2023). The true rate of events like GRB 221009A remains nevertheless difficult to estimate because the Earth is rarely within their beam and we have a single case.

This model, however, does not explain the nondetection of GRBs as apparently energetic as GRB 221009A at higher redshifts. According to the estimate above, there are about 2000 times more GRBs within $z = 6.3$ than within $z = 0.151$. It is thus surprising that the only GRB with E_{iso} beyond 10^{55} erg was found so close to the Earth. This has prompted some authors to investigate alternative ways to explain the BOAT. One such way is the gravitational lensing by an intervening stellar object. This possibility was studied by J. S. Bloom (2022), motivated by the low galactic latitude of GRB 221009A. His study eventually showed that the probability of lensing is very small and significantly lower than the probability of observing a burst like GRB 221009A just by chance. Another approach has been taken by J. Finke & S. Razzaque (2024), who speculate on the existence of a population of nearby narrow-jet GRB population (BOAT-like GRBs), that are supposed to be present only below $z \approx 0.38$. Considering their high beaming and local origin, GRBs from this population would be detected at the rate of ≈3 per century.

The general consensus, however, is that GRB 221009A was a classical long and energetic GRB, whose occurrence close to

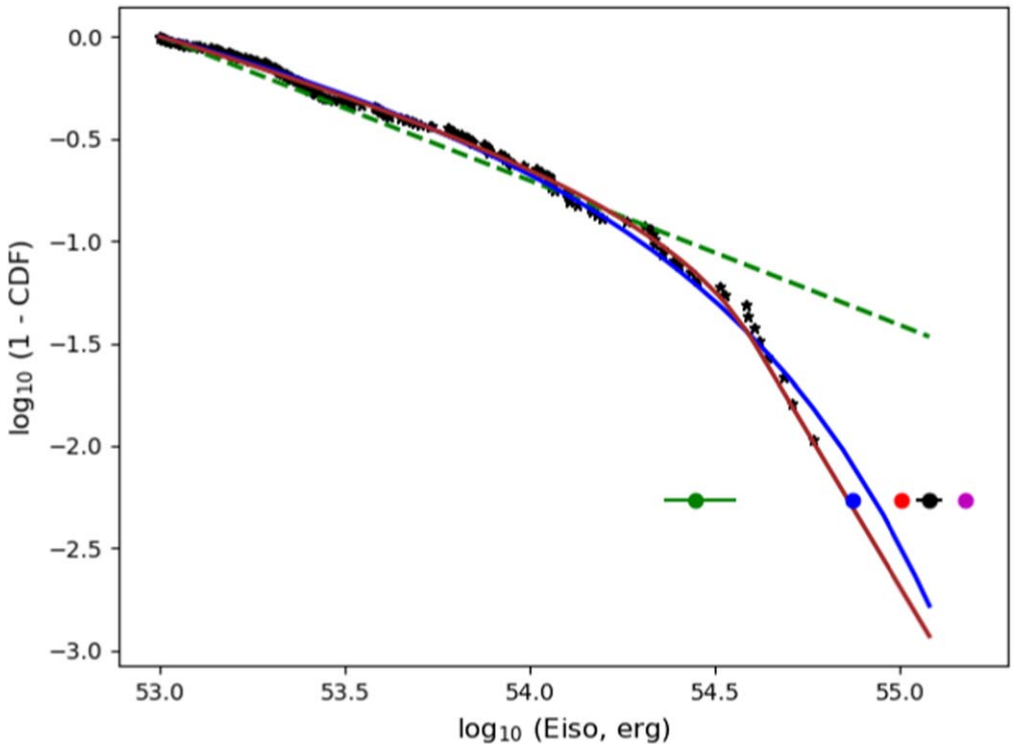

Figure 2. Complementary cumulative energy distribution (CCDF = 1 − CDF) of 185 GRBs, including GRB 221009A. The green, blue, red, black, and magenta points show the isotropic equivalent energy of GRB 221009A, measured by GRBAlpha (J. Řípa et al. 2023), SIRI-2 (L. J. Mitchell et al. 2025), Fermi (S. Lesage et al. 2022), Konus (D. Frederiks et al. 2023b), and GECAM (Z.-H. An et al. 2023), respectively. The green dashed line, the blue solid, and the brown solid line, respectively, show the best PL, CPL, and BPL fits to the $E_{\rm iso}$ differential distribution.

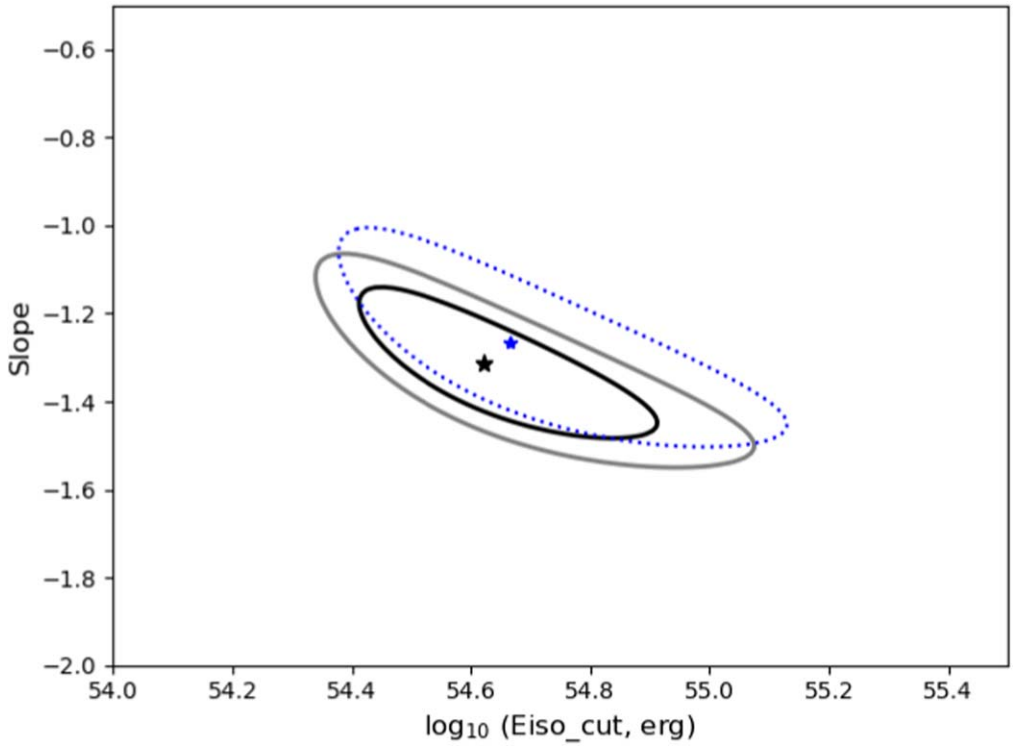

Figure 3. Best-fit parameters for the CPL in a plane showing the slope vs. cutoff energy. The black star shows the best-fit parameters for the sample in this study (with GRB 221009A included in the sample), and the solid contours show the 68 and 90% confidence regions on these parameters. The blue star and dotted blue contour are the best fit and 90% contour for the sample of L. Lan et al. (2023) restricted to GRBs with $E_{\rm iso} \geqslant 10^{53}$ erg.

us was a rare and lucky opportunity. Under this assumption, we now discuss briefly the possible origin of the $E_{\rm iso}$ cutoff.

4.2. Origin of the Energy Cutoff

Various authors (A17; A. Tsvetkova et al. 2017; L. Lan et al. 2023) have shown that apparently very energetic GRBs (close to the $E_{\rm iso}$ cutoff) do not seem to exhibit special properties of their prompt emission, like their duration or their position in the $E_{\rm peak}$–$E_{\rm iso}$ diagram (where $E_{\rm peak}$ is the peak energy of the spectral energy distribution measured at the source, L. Amati et al. 2009). While they often exhibit significant GeV emission, this emission seems to be the simple consequence of their large isotropic equivalent energy at keV–MeV energies (M. Ajello et al. 2019; Sánchez-Ramìrez et al. 2024). Overall, apparently very energetic GRBs appear as the high-energy end of the LGRB population, a conclusion that also applies to GRB 221009A, as discussed in Z.-H. An et al. (2023), E. Burns et al. (2023), D. Frederiks et al. (2023b), D. A. Kann et al. (2023), S. Lesage et al. (2023), J. Řípa et al. (2023), M. Tavani et al. (2023), and H. Sears et al. (2024).

In these conditions, we propose below a short generic discussion on the origin of the $E_{\rm iso}$ cutoff or break, within the framework of the collapsar model of GRBs. We note that other explanations have been proposed in the context of other models; see for instance the work of S. Dado & A. Dar (2022) for the cannonball model, but they are not addressed here. The collapsar model involves a central engine (a black hole (BH) or a magnetar) created by the collapsing core of a massive star that is capable of launching transient ultrarelativistic jets sufficiently energetic to pierce the star's envelope without losing a significant fraction of their energy (see, e.g., S. E. Woosley & J. S. Bloom 2006; O. Bromberg et al. 2011). One crucial ingredient of these models is the large angular momentum of the stellar core needed to avoid its direct collapse into the BH and permit the creation of a temporary accretion disk (A. I. MacFadyen & S. E. Woosley 1999). The isotropic energy can be written as the product of E_γ, the true energy released in gamma rays by the jet emerging from the central engine, and the beaming factor $f_{\rm b}$. The beaming factor is the ratio of the flux emitted in our direction to the flux averaged over the whole sky. For a uniform jet, $f_{\rm b} = 4\pi/\Omega_{\rm j}$, where $\Omega_{\rm j}$ is the solid angle of the jet.

$$E_{\rm iso} = E_\gamma \times f_{\rm b}. \quad (1)$$

The cutoff of the $E_{\rm iso}$ distribution requires a limitation on both quantities: the beaming factor and the energy released by the jet in gamma rays, we briefly discuss these two quantities below.

While the isotropic energy covers a large interval of more than four orders of magnitude (from 10^{51} to 10^{55} erg, for classical LGRBs), E_γ appears limited to a narrower interval of one or two orders of magnitude around 10^{50} erg (D. A. Frail et al. 2001; W. Zhao et al. 2020). If the diversity in $E_{\rm iso}$ values is mostly the result of different jet opening angles, the 3–4 orders of magnitude ratio between $E_{\rm iso}$ and E_γ corresponds to a jet opening angle of about 1°. Indeed, the study of GRBs with the highest $E_{\rm iso}$ suggests that they have beaming factors of the order of 10^3, corresponding to $\theta \approx 2.^\circ5$ and $E_\gamma \geqslant 10^{51}$ erg (see for instance the discussion in Section 4.2 of A17). Compared with these values, the beaming factor of GRB 221009A is still an order of magnitude larger, explaining its remarkable apparent energy with a rather typical E_γ. The $E_{\rm iso}$ cutoff calls for an upper limit on $f_{\rm b}$ ($f_{\rm b} \leqslant 10^3$), suggesting the existence of a minimum jet opening angle of about 1°. We speculate that below this value the jet could simply not form or be subject to destructive instabilities during its propagation.

Turning now to E_γ, it is the product of the jet energy $E_{\rm j}$ by $\eta_{\rm j}$, the radiative efficiency of the jet.

$$E_\gamma = E_{\rm j} \times \eta_{\rm j}. \quad (2)$$

Assuming that GRBs close to the $E_{\rm iso}$ cutoff typically have $f_{\rm b} \approx 1000$ and $\eta_{\rm j} \approx 0.2$, we can evaluate their jet power as $E_{\rm j} \approx 210^{52}$ erg.[5] The observed cutoff would thus imply a limitation of the jet energy around this value. In this context, it is interesting to note some theoretical limitations on the energy of relativistic jets produced by fast-rotating magnetars or protomagnetars and those produced by stellar-mass spinning BHs. According to B. D. Metzger et al. (2011), the maximum power of magnetar-powered jets is limited to $E_\gamma \sim 10^{51}$ erg. Regarding stellar-mass BH jets, the efficiency of the Blandford–Znajek mechanism (R. D. Blandford & R. L. Znajek 1977), which is commonly invoked to extract the BH rotation energy and power GRB jets, strongly depends on the strength of the magnetic field and on the BH spin. It has been shown recently that the angular momentum extracted by the BZ mechanism is very efficient in reducing the BH spin (J. Jacquemin-Ide et al. 2024), leading to a limitation of the jet power, which cannot exceed 1%–2% of the accretion energy, leading to $E_{\rm j,max} \leqslant$ few10^{52} (e.g., Z.-F. Wu et al. 2024). We speculate that the theoretical limitations on the power of the jets generated by the spinning magnetar model or the spinning BH model may explain the observed $E_{\rm iso}$ cutoff.

In any case, the final elucidation of the origin of the cutoff will require more observations of these rare apparently superenergetic events and detailed simulations of jet production and propagation, which are beyond the scope of this paper.

5. Conclusions

We have revisited the bright end of the GRB isotropic equivalent energy distribution, after the detection of GRB 221009A. The main conclusions of our study are the following:

1. GRB 221009A appears as a classical LGRB, albeit with extreme apparent energy. This extreme apparent energy can be attributed to the geometry of its jet, which is among the narrowest detected so far. The lack of GRBs similar to GRB 221009A at larger redshifts remains an open question, considering the small volume enclosed within $z = 0.151$, compared to the volume explored with bright GRBs. With a single event, we cannot decide if GRB 221009A was a highly unprobable, unique detection or if it belongs to a relatively nearby hypothetical population of narrow-jet GRBs, which makes the production of such GRBs more frequent at small redshifts.
2. The detection of GRB 221009A does not invalidate the existence of a cutoff around $E_{\rm iso} = 4 \times 10^{54}$ erg. The interpretation of this cutoff involves a limitation of the jet power combined with a dearth of ultranarrow jets ($\theta_{\rm j} < 1^\circ$). While the first point is a generic prediction of GRB models, the second could be due to an intrinsic lack of ultranarrow jets or their inability to successfully pierce the stellar envelope and still propagate over large

[5] We note an error on the exponent of $E_{\rm jet}$ in Section 4.2 of A17, which should read 10^{52} instead of 10^{51}, we apologize for this mistake.

distances without being destroyed by various instabilities. Detailed simulations of jet formation and propagation will be needed to test these two points.

From an observational perspective, it is also crucial to increase the current sample. In this respect, the successful launch of SVOM (J. Wei et al. 2016; J. L. Atteia et al. 2022) on 2024 June 22, should improve the situation in the coming years, with its capacity to provide both fast positions à la Swift and broadband spectra of the prompt emission à la Fermi/GBM.

Acknowledgments

The authors acknowledge the use of the J. Greiner GRB page (https://www.mpe.mpg.de/ jcg/grbgen.html) to build the list of GRBs with $E_{\rm iso} \geqslant 10^{53}$ erg used in this study. We thank the referee for comments that led us to clarify various points of the article.

Facilities: Fermi, Wind, VLT:Antu, VLT:Kuyen.

Software: astropy (Astropy Collaboration et al. 2013, 2018).

ORCID iDs

Jean-Luc Atteia https://orcid.org/0000-0001-7346-5114
Jean-Pascal Dezalay https://orcid.org/0009-0004-9396-5270
Francis Fortin https://orcid.org/0000-0003-3642-2267
Olivier Godet https://orcid.org/0000-0001-7635-9544
Sébastien Guillot https://orcid.org/0000-0002-6449-106X
Alain Klotz https://orcid.org/0000-0002-2652-0069
Robert Mochkovitch https://orcid.org/0000-0001-8588-8499
Damien Turpin https://orcid.org/0000-0003-1835-1522

References

Ajello, M., Arimoto, M., Axelsson, M., et al. 2019, ApJ, 878, 52
Amati, L., Frontera, F., & Guidorzi, C. 2009, A&A, 508, 173
An, Z.-H., Antier, S., Bi, X.-Z., et al. 2023, arXiv:2303.01203
Aptekar, R. L., Frederiks, D. D., Golenetskii, S. V., et al. 1995, SSRv, 71, 265
Astropy Collaboration, Robitaille, T. P., Tollerud, E. J., et al. 2013, A&A, 558, A33
Astropy Collaboration, Price-Whelan, A. M., Sipőcz, B. M., et al. 2018, AJ, 156, 123
Atteia, J. L., Cordier, B., & Wei, J. 2022, IJMPD, 31, 2230008
Atteia, J. L., Heussaff, V., Dezalay, J. P., et al. 2017, ApJ, 837, 119
Atteia, J. L., Kawai, N., Vanderspek, R., et al. 2005, ApJ, 626, 292
Beniamini, P., & Nakar, E. 2019, MNRAS, 482, 5430
Bissaldi, E., Lesage, S. & Fermi GBM Team 2020, GCN, 27930, 1
Blanchard, P. K., Villar, V. A., Chornock, R., et al. 2024, NatAs, 8, 774
Blandford, R. D., & Znajek, R. L. 1977, MNRAS, 179, 433
Bloom, J. S. 2022, RNAAS, 6, 220
Bright, J. S., Rhodes, L., Farah, W., et al. 2023, NatAs, 7, 986
Bromberg, O., Nakar, E., Piran, T., & Sari, R. 2011, ApJ, 740, 100
Burns, E., Svinkin, D., Fenimore, E., et al. 2023, ApJL, 946, L31
Cao, Z., Aharonian, F., An, Q., et al. 2023, SciA, 9, eadj2778
Castro-Tirado, A. J., Hu, Y., Fernandez-Garcia, E., et al. 2019, GCN, 23708, 1
Castro-Tirado, A. J., Valeev, A. F., Vinokurov, A., et al. 2022, GCN, 31423, 1
Cenko, S. B., Frail, D. A., Harrison, F. A., et al. 2010, ApJ, 711, 641
Curran, P. A., Wijers, R. A. M. J., Heemskerk, M. H. M., et al. 2008, A&A, 490, 1047
Dado, S., & Dar, A. 2022, ApJL, 940, L4
D'Avanzo, P., Bolmer, J., D'Elia, V., et al. 2018a, GCN, 22555, 1
D'Avanzo, P., Heintz, K. E., de Ugarte Postigo, A., et al. 2018b, GCN, 23246, 1
de Ugarte Postigo, A., Agui Fernandez, J. F., Thoene, C. C., & Izzo, L. 2023, GCN, 34409, 1
de Ugarte Postigo, A., Kann, D. A., Thoene, C. C., Blazek, M., & Agui Fernandez, J. F. 2021a, GCN, 29320, 1
de Ugarte Postigo, A., Kann, D. A., Thoene, C., et al. 2021b, GCN, 30272, 1
de Ugarte Postigo, A., Thoene, C., Agui Fernandez, J. F., et al. 2021c, GCN, 30194, 1
de Ugarte Postigo, A., Thöne, C. C., Bolmer, J., et al. 2018, A&A, 620, A119
Finke, J., & Razzaque, S. 2024, ApJ, 975, 70
Frail, D. A., Kulkarni, S. R., Sari, R., et al. 2001, ApJL, 562, L55
Frederiks, D., Golenetskii, S., Aptekar, R., et al. 2016, GCN, 20111, 1
Frederiks, D., Golenetskii, S., Aptekar, R., et al. 2018a, GCN, 22546, 1
Frederiks, D., Golenetskii, S., Aptekar, R., et al. 2018b, GCN, 23011, 1
Frederiks, D., Golenetskii, S., Aptekar, R., et al. 2018c, GCN, 23240, 1
Frederiks, D., Golenetskii, S., Aptekar, R., et al. 2019a, GCN, 24715, 1
Frederiks, D., Golenetskii, S., Aptekar, R., et al. 2019b, GCN, 26576, 1
Frederiks, D., Golenetskii, S., Aptekar, R., et al. 2020a, GCN, 29084, 1
Frederiks, D., Golenetskii, S., Aptekar, R., et al. 2020b, GCN, 29150, 1
Frederiks, D., Golenetskii, S., Lysenko, A., et al. 2021a, GCN, 30196, 1
Frederiks, D., Golenetskii, S., Lysenko, A., et al. 2021b, GCN, 30366, 1
Frederiks, D., Golenetskii, S., Lysenko, A., et al. 2021c, GCN, 30694, 1
Frederiks, D., Lysenko, A., Ridnaya, A., et al. 2022a, GCN, 32295, 1
Frederiks, D., Lysenko, A., Ridnaya, A., et al. 2022b, GCN, 31511, 1
Frederiks, D., Lysenko, A., Ridnaia, A., et al. 2023a, GCN, 34403, 1
Frederiks, D., Svinkin, D., Lysenko, A. L., et al. 2023b, ApJL, 949, L7
Frederiks, D. D., Hurley, K., Svinkin, D. S., et al. 2013, ApJ, 779, 151
Fulton, M. D., Smartt, S. J., Rhodes, L., et al. 2023, ApJL, 946, L22
Fynbo, J. P. U., de Ugarte Postigo, A., D'Elia, V., et al. 2018, GCN, 23356, 1
Fynbo, J. P. U., de Ugarte Postigo, A., Xu, D., et al. 2022, GCN, 31359, 1
Gehrels, N., Chincarini, G., Giommi, P., et al. 2004, ApJ, 611, 1005
Gupta, R., Gupta, S., Chattopadhyay, T., et al. 2022, MNRAS, 511, 1694
Hjorth, J., Møller, P., Gorosabel, J., et al. 2003, ApJ, 597, 699
Izzo, L., D'Elia, V., de Ugarte Postigo, A., et al. 2022, GCN, 32291, 1
Izzo, L., de Ugarte Postigo, A., Kann, D. A., et al. 2018, GCN, 23488, 1
Jacquemin-Ide, J., Gottlieb, O., Lowell, B., & Tchekhovskoy, A. 2024, ApJ, 961, 212
Kann, D. A., Agayeva, S., Aivazyan, V., et al. 2023, ApJL, 948, L12
Kong, D.-F., Wang, X.-G., Zheng, W., et al. 2024, ApJ, 971, 56
Krühler, T., Malesani, D., Fynbo, J. P. U., et al. 2015, A&A, 581, A125
Kulkarni, S. R., Djorgovski, S. G., Ramaprakash, A. N., et al. 1998, Natur, 393, 35
Lan, L., Gao, H., Li, A., et al. 2023, ApJL, 949, L4
Laskar, T., Alexander, K. D., Margutti, R., et al. 2023, ApJL, 946, L23
Lesage, S., Meegan, C. & Fermi Gamma-Ray Burst Monitor Team 2022, GCN, 31360, 1
Lesage, S., Veres, P., Briggs, M. S., et al. 2023, ApJL, 952, L42
LHAASO Collaboration, Cao, Z., Aharonian, F., et al. 2023, Sci, 380, 1390
Lysenko, A., Frederiks, D., Ridnaia, A., et al. 2022, GCN, 32152, 1
MacFadyen, A. I., & Woosley, S. E. 1999, ApJ, 524, 262
Maiorano, E., Masetti, N., Palazzi, E., et al. 2006, A&A, 455, 423
Malesani, D. B., Levan, A. J., Izzo, L., et al. 2023, arXiv:2302.07891
Malesani, D. B., Vielfaure, J. B., Izzo, L., et al. 2020, GCN, 29100, 1
Meegan, C., Lichti, G., Bhat, P. N., et al. 2009, ApJ, 702, 791
Metzger, B. D., Giannios, D., Thompson, T. A., Bucciantini, N., & Quataert, E. 2011, MNRAS, 413, 2031
Mitchell, L. J., Finke, J. D., Phlips, B., Johnson, W. N., & Kong, E. 2025, ApJ, 979, 153
O'Connor, B., Troja, E., Ryan, G., et al. 2023, SciA, 9, eadi1405
Palmerio, J., Malesani, D. B., Fynbo, J. P. U., et al. 2022, GCN, 31480, 1
Pankov, N. S., Pozanenko, A. S., Minaev, P. Y., et al. 2023, AstL, 49, 81
Planck Collaboration, Ade, P. A. R., Aghanim, N., et al. 2014, A&A, 571, A16
Poolakkil, S., Meegan, C. & Fermi GBM Team 2023, GCN, 33288, 1
Poolakkil, S., Preece, R., Fletcher, C., et al. 2021, ApJ, 913, 60
Ren, J., Wang, Y., Zhang, L.-L., & Dai, Z.-G. 2023, ApJ, 947, 53
Rhoads, J. E. 1997, ApJL, 487, L1
Ridnaia, A., Golenetskii, S., Aptekar, R., et al. 2020, GCN, 28323, 1
Ridnaia, A., Frederiks, D., Lysenko, A., et al. 2022, GCN, 31429, 1
Rossi, A., Frederiks, D. D., Kann, D. A., et al. 2022, A&A, 665, A125
Saccardi, A., Kann, D. A., Palmerio, J., et al. 2023, GCN, 33281, 1
Sakamoto, T., Lamb, D. Q., Kawai, N., et al. 2005, ApJ, 629, 311
Sánchez-Ramìrez, Lang, R. G., Pozanenko, A., et al. 2024, A&A, 692, A3
Sato, Y., Murase, K., Ohira, Y., & Yamazaki, R. 2023, MNRAS, 522, L56
Savchenko, V., Ubertini, P., Bazzano, A., et al. 2024, A&A, 684, L2
Schady, P., Xu, D., Heintz, K. E., et al. 2019, GCN, 23632, 1
Schwarz, G. 1978, AnSta, 6, 461
Sears, H., Chornock, R., Blanchard, P., et al. 2024, arXiv:2412.02663
Shrestha, M., Sand, D. J., Alexander, K. D., et al. 2023, ApJL, 946, L25
Srinivasaragavan, G. P., O'Connor, B., Cenko, S. B., et al. 2023, ApJL, 949, L39
Svinkin, D., Golenetskii, S., Aptekar, R., et al. 2018, GCN, 23495, 1
Svinkin, D., Golenetskii, S., Aptekar, R., et al. 2019, GCN, 25974, 1

Svinkin, D., Golenetskii, S., Aptekar, R., et al. 2020a, GCN, 27867, 1
Svinkin, D., Golenetskii, S., Aptekar, R., et al. 2020b, GCN, 28872, 1
Svinkin, D., Golenetskii, S., Frederiks, D., et al. 2021, GCN, 30276, 1
Tanvir, N., Rossi, A., Xu, D., et al. 2021, GCN, 30771, 1
Tavani, M., Piano, G., Bulgarelli, A., et al. 2023, ApJL, 956, L23
Thoene, C. C., de Ugarte Postigo, A., Agui Fernandez, J. F., et al. 2023, GCN, 35373, 1
Tsvetkova, A., Frederiks, D., Lysenko, A., et al. 2022, GCN, 31433, 1
Tsvetkova, A. & KW Team 2022, GCN, 31436, 1
Tsvetkova, A., Frederiks, D., Golenetskii, S., et al. 2017, ApJ, 850, 161
Tsvetkova, A., Frederiks, D., Svinkin, D., et al. 2021, ApJ, 908, 83
Tsvetkova, A., Golenetskii, S., Aptekar, R., et al. 2018, GCN, 23363, 1
Tsvetkova, A., Golenetskii, S., Aptekar, R., et al. 2019, GCN, 23637, 1
Ursi, A., Tavani, M., Frederiks, D. D., et al. 2020, ApJ, 904, 133
Vielfaure, J. B., Arabsalmani, M., Heintz, K. E., et al. 2019, GCN, 26553, 1
Vielfaure, J. B., Izzo, L., Xu, D., et al. 2020a, GCN, 29077, 1
Řípa, J., Takahashi, H., Fukazawa, Y., et al. 2023, A&A, 677, L2
Vielfaure, J. B., Vergani, S. D., Japelj, J., et al. 2020b, A&A, 641, A30
Vreeswijk, P. M., Kann, D. A., Heintz, K. E., et al. 2018, GCN, 22996, 1
Wei, J., Cordier, B., Antier, S., et al. 2016, arXiv:1610.06892
Williams, M. A., Kennea, J. A., Dichiara, S., et al. 2023, ApJL, 946, L24
Woosley, S. E., & Bloom, J. S. 2006, ARA&A, 44, 507
Wu, Z.-F., Damoulakis, M., Beniamini, P., & Giannios, D. 2024, arXiv:2411.12850
Xu, D., Izzo, L., de Ugarte Postigo, A., et al. 2021, GCN, 30357, 1
Xu, D., Vielfaure, J. B., Kann, D. A., et al. 2020, GCN, 28847, 1
Xu, D., Zhu, Z. P., Izzo, L., et al. 2022, GCN, 32141, 1
Yang, J., Zhao, X.-H., Yan, Z., et al. 2023, ApJL, 947, L11
Yao, Y., Miller, A., Ho, A., & Perley, D. 2021, GCN, 29673, 1
Zhang, B. T., Murase, K., Ioka, K., et al. 2023, ApJL, 947, L14
Zhao, W., Zhang, J.-C., Zhang, Q.-X., et al. 2020, ApJ, 900, 112
Zhu, Z. P., Izzo, L., Fu, S. Y., et al. 2021, GCN, 30692, 1